ORIGINAL ARTICLE

A TOpti simulation for finding fuel saving by optimising propulsion control and power management

Miikka Jaurola[1] · Anders Hedin[2] · Seppo Tikkanen[1] · Kalevi Huhtala[1]

Abstract

The optimisation of load shares between parallel power sources is essential for fuel-efficient propulsion systems. A more complete power management problem can be formulated by including the propeller and its propulsion control. Not only does this allow for a reduction in the propeller load under the changing operating conditions of the vessel, but also it enables the minimisation of the machinery's fuel consumption at load- and speed-dependent efficiency models. The need to optimise the design of the machinery in marine vessels has motivated the authors of the current article to develop a design tool for this purpose. The present case study gives an overview of the tool's features and compares the optimal power management of a fishing boat with different propulsion control variants. Compared with a controllable pitch propeller, which is operated at a fixed speed, reductions in fuel consumption were achieved with reduced propeller speeds. The best fuel savings, approximately 11%, were achieved using a two-speed gearbox with a controllable pitch propeller.

Keywords Propulsion control · Energy-efficient propulsion · Numerical optimisation · Power management · Fishing boat

Abbreviations

AC	Alternate current
BSFC	Brake-specific fuel consumption (g/kWh)
COBYLA	Constrained optimisation by linear approximations
CPP	Controllable pitch propeller
DE	Diesel electric topology
DM	Diesel mechanical topology
DC	Direct current
E-GRID	Onboard electric grid
GB	Gearbox
GEN	Genset
LT	Local time optimisation method
M/G	Electric motor/generator
ME	Main engine
MCR	Maximum continuous rate (W)
PTI	Power take-in
PTO	Power take-off
VFD	Variable frequency drive

List of symbols

$\Delta \dot{m}$	Total fuel consumption rate error (kg/h)
Δn	Propeller speed error (rpm)
$\Delta P_{M/G}$	Optimal control error for M/G (kW)
Δt	Instantaneous time step length (s)
η_{GEN}	Efficiency of the GEN (–)
$\eta_{M/G}$	Efficiency of the M/G (–)
C_R	Ship hull resistance coefficient [N s/m]
D	Diamater of the propeller (m)
J	Advance number (–)
k	Integer exponent for the ship's velocity (–)
$K_{c_{GEN}}$	Internal loss coefficient of generator unit in the GEN (–)
$K_{c_{M/G}}$	Internal loss coefficient of the M/G (–)
$K_{GB_{ME}}$	Gearbox loss coefficient for the ME (–)
$K_{GB_{M/G}}$	Gearbox loss coefficient for the M/G (–)
K_Q	Torque coefficient of the propeller (–)
K_T	Thrust coefficient of the propeller (–)
n	Rotational speed of the propeller (1/s)
P_{GEN}	Operating power of the GEN (W)
P_{ME}	Operating power of the ME (W)
$P_{hotel,t}$	Hotel load (W)
$P_{prop,t}$	Propeller load (W)
$P_{M/G}$	Operating power of the M/G (W)
$\hat{P}_{GEN}$	Scaled operating power of the GEN (–)
$\hat{P}_{ME}$	Scaled operating power of the ME (–)
$\hat{P}_{M/G}$	Scaled operating power of the M/G (–)

✉ Miikka Jaurola
miikka.jaurola@tuni.fi

1   Unit of Automation Technology and Mechanical Engineering, Tampere University, Tampere, Finland

2   Wärtsilä Norway AS, Rubbestadneset, Norway

P/D	Pitch per diameter ratio of the propeller (–)
Q	Propeller torque (Nm)
R	Ship hull resistance (N)
T	Propeller thrust (N)
t	Instantaneous time (s)
u	Discretised control for the component (–)
V	Ship speed (m/s)

1 Introduction

The increasingly strict emission legislation and drive towards reduced operational costs have motivated maritime engineers to design efficient propulsion systems and operate the machinery in an optimal way. From the perspective of energy efficiency, we should not focus on the optimal design of individual components alone. Instead, the whole ship's power system, from the power sources to what is consuming power, must be considered. Optimal power management is at the epicentre of the design problem for optimal ship machinery. As power systems become more complex, the more variables are introduced into the optimisation problem, and the more challenging optimising the power management becomes. When it comes to the state of the art in optimal design of hybrid electric boats and their power and energy management, the literature reviews in [1] and [2] discuss the research articles from various authors.

By introducing a propeller in the power system model, the frame of the design and power management optimisation problem can be expanded. Besides load sharing and load levelling, one can now also study reducing the propulsion load itself. In other words, can the propeller be operated at a higher efficiency to improve the overall energy use in the system? Hence, the choices for the propeller type and control affect where the optimal load share is found.

The current article continues a description of the features of TOpti [3]: a simulation and optimisation framework developed for maritime engineers by the authors of the current article. In the current study, we are comparing how the different ship operating points translate into the operating points in machinery with different propeller types. A conventional fixed pitch propeller is compared with a controllable pitch propeller, which is operated at a fixed speed, multiple discrete speeds and a continuously variable speed. As a case study, the fuel consumption of a fishing boat is studied under different propulsion control variants. The machinery usage is optimised to minimise the fuel consumption over a generic duty cycle. Although more complex machinery configurations, such as parallel hybrids with battery energy storage systems, can be simulated with TOpti, the current study focuses on the propeller operating points of a combined diesel-mechanical and/or diesel-electric propulsion system with a PTI/PTO gearbox. In this way, the time-dependent

factors, such as the charge and discharge strategy of a battery with a finite capacity, will not influence the optimal solution.

The current article is organised as follows: The system modelling techniques are described in Sect. 2. This is followed by a briefing on the optimisation methodology and the formulation of the optimisation problem in Sect. 3. A more detailed description of the simulation and optimisation methods used in TOpti can be found in [3]. The simulation results are discussed in Sect. 4 and validated with an exhaustive search algorithm.

2 Modelling the power system for the studied fishing boat

This section presents the system modelling methods used in the case study. The simulation framework—TOpti—is aimed at the engineers who are responsible for system integration in ship power systems. Rather than trying to capture the small details and obtaining absolute accuracy in the system models, TOpti was developed to make relative comparisons of system candidates for the baseline designs early on in the process. Therefore, simplified and static modelling techniques with quasi-static time scales in the duty cycle are considered to be sufficient. In addition, the simple models reduce the computational workload of the optimisation algorithm, thus allowing us to widen the frame of the studied problem.

Because the focus in the current article is on the different propulsion concepts, the principles of propeller modelling are described first in Sect. 2.1. This is followed by introducing the compared machinery topology variants and the fishing boat duty cycle in Sect. 2.2. To conclude this modelling section, the modelling techniques for the individual machinery components are then described.

2.1 Propulsion control in fishing boats

The current article studies the fuel savings that are gained from achieving the optimal usage of different propulsion configurations for a fishing boat. The four propulsion control variants in Fig. 1 are compared as follows: Variant (a) is a fixed-speed CPP. Variant (b) has a conventional FPP to generate thrust. Variant (c) has the same propeller as in (a), but now, the gearbox has two reduction speeds for the propeller shaft. Variant (d) has mechanically the same configuration as (a), but here, the propulsion control is handled by two independent variables: the propeller pitch and the rotational speed. Variants (a) and (b) have a single equilibrium point for a given vessel's operating point. Variant (c) has two discrete equilibrium points for each vessel's operating point: one for both propeller speeds. Variant (d), on the other hand, has an infinite number of equilibrium points that are defined
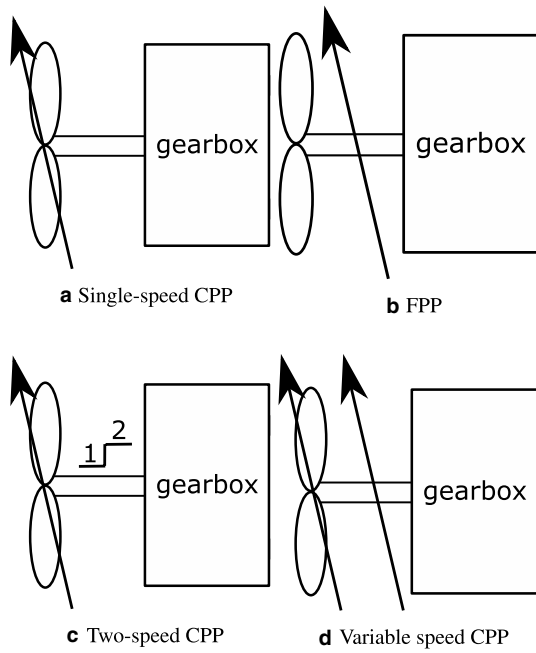
a Single-speed CPP

b FPP

c Two-speed CPP

d Variable speed CPP

Fig. 1 Studied propulsion control variants

by the combination of the propeller blade pitch and propeller speed.

The propellers for the current article were modelled using Eqs 1a–1e, where the thrust coefficient K_T and the torque coefficients K_Q are described as a function of the advance number J (Eqs. 1a and 1b, respectively). The third-order polynomial curves of these coefficients were estimated using the Wageningen B5-75 screw series propeller curves shown in [4]. Eqs. 1c and 1d describe the thrust generated by the propeller, T, and the torque, which affects the propeller shaft, Q. A simplified power equilibrium was used, which

excluded the wake deductions for the water velocity, that enters the propeller. Thus, the open water efficiency of the propeller, η_0, was used to model the ratio of the output and input powers, which is shown in Eq. 1e. Here, the output power is the power needed to move the vessel hull at the requested velocity V, and the input power is the propeller's shaft power.

$$K_T = c_{T0} + c_{T1} \cdot J + c_{T2} \cdot J^2 + c_{T3} \cdot J^3 \tag{1a}$$

$$K_Q = c_{Q0} + c_{Q1} \cdot J + c_{Q2} \cdot J^2 + c_{Q3} \cdot J^3 \tag{1b}$$

$$T = K_T \cdot \rho \cdot n^2 \cdot D^4 \tag{1c}$$

$$Q = K_Q \cdot \rho \cdot n^2 \cdot D^5 \tag{1d}$$

$$\eta_0 = \frac{K_T \cdot J}{K_Q \cdot 2\pi} = \frac{T \cdot V}{Q \cdot 2\pi \cdot n} \tag{1e}$$

The K_T, K_Q and efficiency curves for the studied propellers are shown in Fig. 2. The propeller diameter is set to 4.5 m for both propeller types. The pitch per diameter (P/D) ratio of an FPP is set to 0.6. A higher P/D value would move the equilibrium points towards lower rotational speeds, which, in turn, would violate the maximum power curve of the machinery when at higher propulsion loads. The pitch angle mechanism requires space inside the CPP hub. Therefore, the FPP with an equal diameter has a larger effective blade area and, thus, slightly better thrust characteristics compared with the CPP at P/D = 0.6. In the current study, the difference is approximately 1.5% in favour of the FPP. For the FPP, the static operating points are solved by finding the rotational speed, which generates thrust to match the
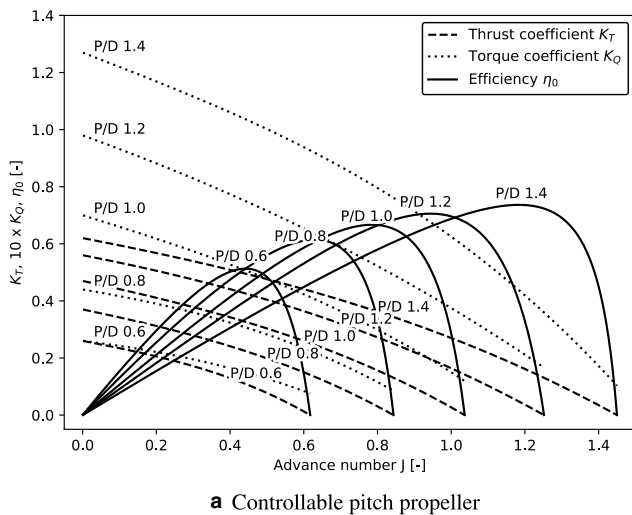
a Controllable pitch propeller
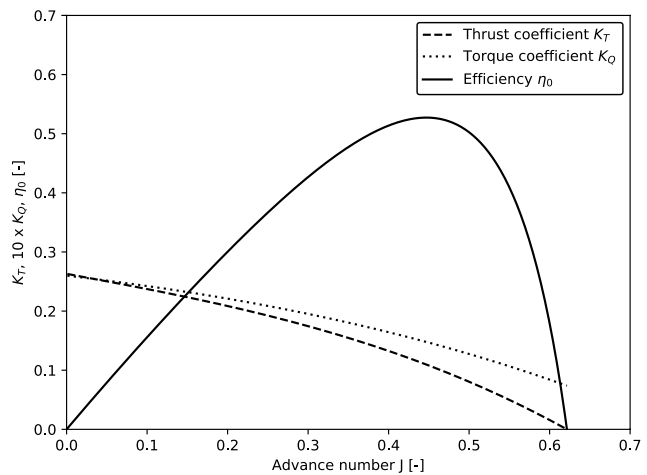
b Fixed pitch propeller, P/D=0.6

Fig. 2 Characteristic curves for the modelled propellers

instantaneous resistance from the duty cycle of the fishing boat. For the CPP, the operating points are solved by interpolating between the characteristic curves, shown in Fig. 2. The CPP has a maximum P/D value of 1.35 and a rated speed of 153 rpm.

The resistance, R, which affects the vessel body in water, is modelled using Eq. 2, where C_R is the resistance coefficient, V is the vessel velocity, and k is the integer exponent for the velocity. The equilibrium operating point of the vessel is solved by setting the resistance R to be equal to propeller thrust T. In TOpti, the user can define the resistance coefficient and make it constant throughout the simulation or make it time dependent. Although the pressure resistance is not modelled physically, its effect can be manually lumped in the resistance R by tuning the resistance coefficient C_R manually for each time step in the simulation.

$$R = C_R \cdot V^k \tag{2}$$

2.2 PTI/PTO combines the mechanical and electric propulsion systems

The machineries for the studied fishing boat are shown in Fig. 3. The propulsion system includes the studied propeller variant, which is fed by a PTI/PTO gearbox (GB). The input shaft of the gearbox is powered by the main engine (ME), and the PTI/PTO shaft is connected to an induction-type electric motor–generator (M/G). The M/G is linked to an alternate current (AC) on-board electric grid (E-GRID). The E-GRID has its own independent and external load for the hotel and auxiliary loads (HOTEL/AUX). A diesel generator (GEN) is included in the machinery to make use of a more practical example of a modern-day fishing boat's power system.

For practicality purposes, two machinery topology variants are studied. To maintain a fixed frequency in the AC grid, the PTI/PTO and GEN must operate on the same frequency. Propulsion variants (a) and (c) in Fig. 1 allow for a fixed speed at the engine and PTI/PTO shafts. Therefore, the power system in Fig. 3a does not need an additional variable frequency drive (VFD) to adjust the electric current frequency when mechanical power is converted into electric power in the M/G or vice versa. However, variants (b) and (d) require the addition of a VFD to maintain a fixed grid frequency because the propulsion control requires variable propeller speeds and, therefore, variable PTI/PTO speeds. Figure 3b shows the additional VFD in the machinery and how it is lumped together with the induction motor to present a motor–generator for a variable-speed PTI/PTO. It is assumed that the GEN is always rotating at a fixed speed of 1200 rpm.

An artificial duty cycle is generated for the boat, and it is based on the two main operating modes of a trawler: trawling at a low speed and high resistance and a transit mode that moves at a high speed and with a low resistance. In addition to these two modes, a zero propulsion mode and a low-speed transit mode are included. The duty cycle, which is shown in Fig. 4, defines the vessel velocity, V, vessel resistance coefficient, C_R, and the power demand of HOTEL/AUX during the voyage. The integer exponent $k = 3$ throughout the duty cycle and the same cycle is used for all the studied cases. The simplified and quasi-static duty cycle is split into time steps of 0.5 h.

For the current study, a shut-off is allowed for the ME and GEN at any time. Also, if zero thrust is needed from the propulsion system that has a CPP, the blade pitch is turned to zero. However, the propeller is still required to rotate to stay ready to manoeuvre the boat and avoid free drifting. This means that even at a zero pitch, a CPP consumes power, even though it does not generate thrust.

2.3 Individual machinery component models

The simplified and static modelling approach in the current article incorporated the use of static efficiency interpolation maps for the main components in the machinery. The used efficiency maps are shown in Fig. 5. The brake-specific fuel consumption (BSFC) map of the ME and efficiency maps for the both M/G variants were three dimensional, even though the machinery should be operated at a fixed speed. The shaft speeds in the graphs refer to the component's own shaft speed—not the speed of the propeller. Two dimensional interpolation maps were used with the GEN because it always runs at the rated speed. The main specifications of the machinery are shown in Table 1.

For the M/G and the generator unit in the GEN, the following simplification was made: the conversion losses in the additional power electronic components and the transfer losses in the electric grid were lumped into the efficiency
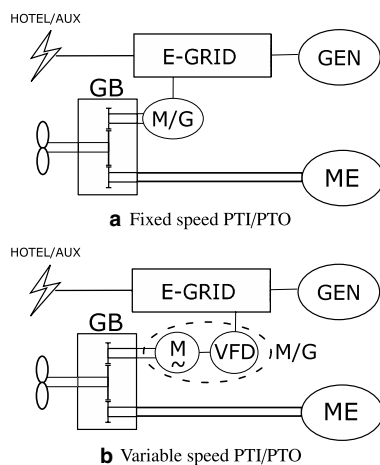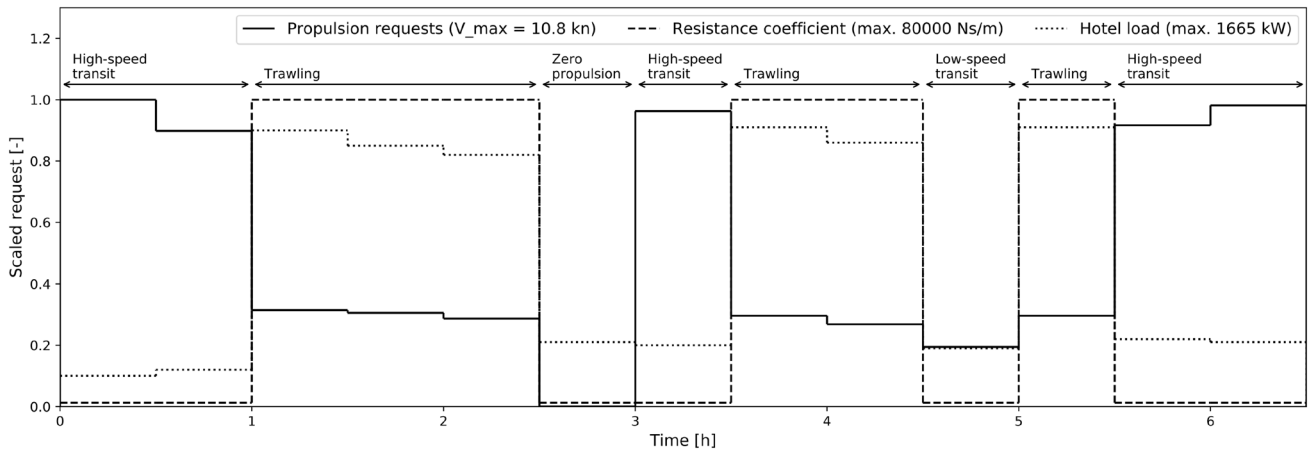

Fig. 3 Studied machinery topologies

Fig. 4 Estimated duty cycle for the studied fishing boat

map of the primary electric unit (i.e., the electric motor or generator). The topologies with a fixed-speed PTI/PTO use the efficiency map with notation A. The topologies with a variable-speed PTI/PTO have the additional VFD unit; therefore, these topologies use a modified efficiency map with notation B to model the M/G efficiency. Otherwise,
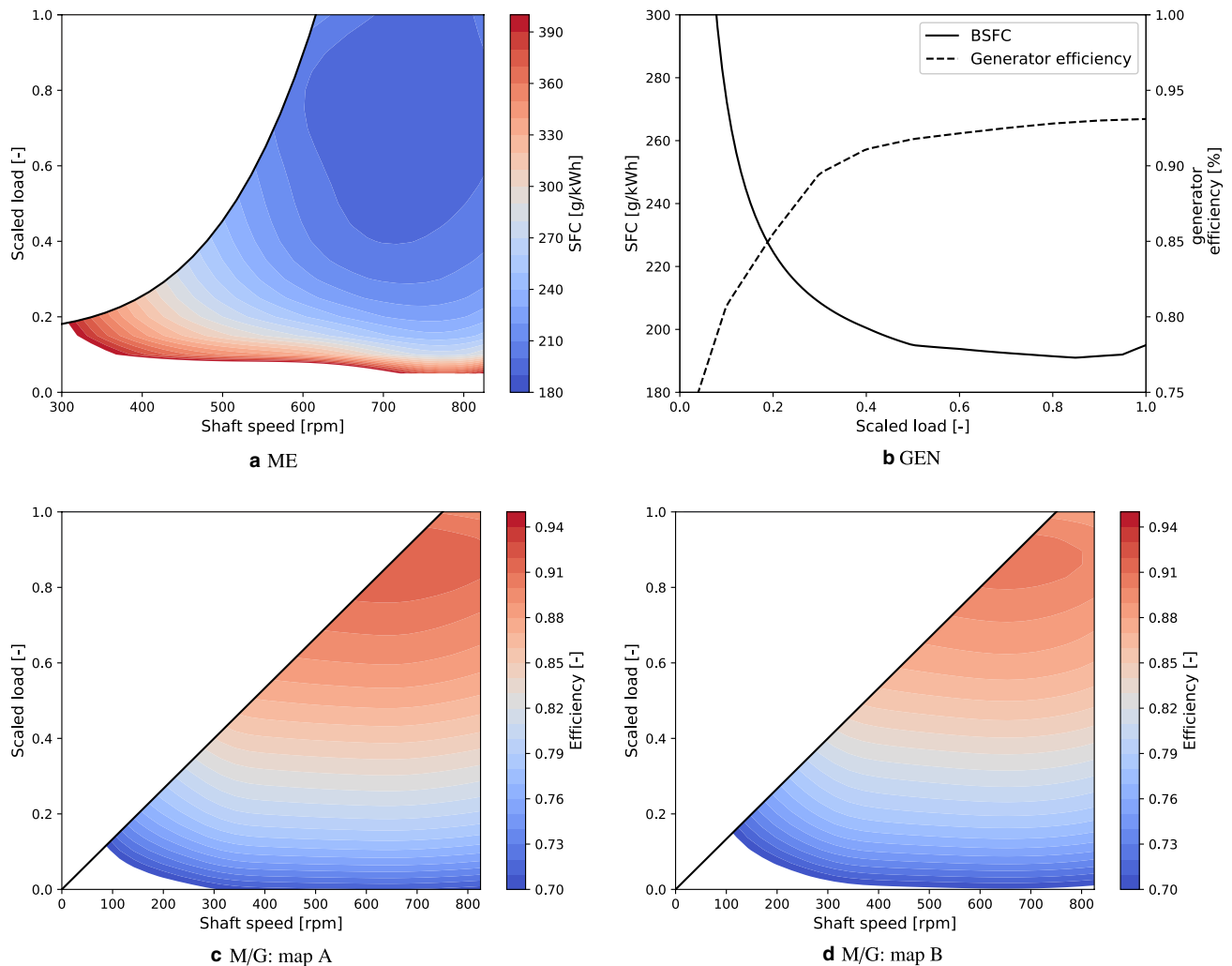

Fig. 5 Efficiency maps of the main components

Table 1 Machinery specifications

Machine	MCR (kW)	Rated speed (rpm)	Other
ME	3480	750	Four-stroke, variable speed
GEN	1665	1200	Four-stroke, fixed speed
M/G	1500	750	Induction motor

the same component models apply to all four propulsion variants.

The gearbox was modelled with two parallel gear contact pairs. The simplified shaft configuration is shown in Fig. 3. Although the main engine and the PTI/PTO shafts run at the same speed, the speed of the propeller shaft was reduced with a gear ratio. For the single-speed gearbox, the reduction ratio was 4.9:1, and for the two-speed gearbox, gear ratios of 4.9:1 and 8.3:1 were used. Each gear contact pair had a fixed efficiency of 98%.

The simulation framework has a quadratic power loss model for the clutch slip in the diesel engines. If the propeller is required to rotate at speeds that would make the diesel engine run below a defined idling speed, the clutch starts to slip. A power loss, which is quadratic to the slip ratio, is generated in the clutch. An example of this type of condition is a requirement for low thrust from an FPP, for example, during manoeuvring.

It must be noted that the machinery component models, propeller included, were not validated by any measurements. As long as the efficiency maps reasonably capture the main effects of the component's operating range, the purpose of assisting in making the early design decisions is achieved. The configurations for the studied propulsion variants are summarised in Table 2.

3 Finding the best machinery usage

In short, the optimisation question in the studied power system focuses on how we should share the load demands between the power sources to minimise the fuel consumption rate of the whole system. To answer this question, a constrained optimisation problem is formulated and solved.

Table 2 Summary of the studied variants

Variant	Propeller	Gearbox	M/G efficiency map
(a)	CPP	Single speed	Map A
(b)	FPP	Single speed	Map B
(c)	CPP	Two speed	Map A
(d)	CPP	Single speed	Map B

The constraints cover the fact that the requested duty cycle is, first of all, completed, but also that the system is maintaining an equilibrium regarding the power. In addition, the constraints ensure that the defined maximum operating limits for different components are not being violated.

The simulations in the current article utilise the same principles for formulating and solving the optimisation problem as described in [3]. Essentially, the optimisation routine is the same for all four system variants. First, the propeller load is calculated for each vessel operating point in the duty cycle. Then, the routine formulates the optimisation problem in a two-layered scheme, which is recapitulated later on this section. Finally, all the constrained search spaces are processed with the chosen algorithm to find the optimal usage for the machinery. In [3], this is called the local time optimisation method (LT), meaning that the control decision is always made based on the current system state. The biggest difference is variant (d), which has a continuously variable-speed CPP: it needs an additional optimisation variable because it has one more variable in its propulsion control compared with the other variants. Here, the rotational speed of the CPP is chosen as the additional optimisation variable; therefore, the propeller load needs to be re-evaluated each time the algorithm evaluates the objective and constraint functions.

The optimisation framework used in the current study combines the use of a discrete search space for the power system operating modes and a gradient-based optimisation algorithm for finding local optima from a set of search spaces. This section briefly describes this two-layered optimisation methodology and the problem formulation for the studied system variants. The discrete search space for the operating modes is discussed first.

In TOpti, each component in the machinery has user-defined operating modes. One can think of these modes as a way to deliver or transfer power. For example, a diesel engine can be in an active mode, noted here with 1, where it delivers mechanical power to a gearbox shaft. The engine can also be in an inactive mode, noted with 0, where it does not deliver power to the gearbox. For another example, an electric motor can work in a motoring mode, a generating mode or in an inactive mode. A motoring mode for an electric motor, noted here with -1, means that the unit is taking power from the electric grid and delivering it to the gearbox. The generating mode, noted with 1, means that power is being delivered in the opposite direction: from the gearbox into the electric grid. The number of modes can be reduced, for example, if the user is only interested in a power management strategy where the electric motor only works in either a motoring or generating mode.

Then, the optimisation routine generates a set of all possible mode combinations that the machinery can work in. This set can be described using an array of system modes, which

is shown in Fig. 6. This figure also illustrates the modes of the individual components within the two example mode combinations. The mode combinations are then checked for their feasibility for each loading condition in the duty cycle. This means that at any given time, the demand for all power consumers must be supplied by the active power sources.

Now, the optimisation routine is ready to start to process all the feasible mode combinations in all the time steps of the duty cycle. This is accomplished by formulating the objective and constraint functions for the optimisation problem and solving the problem with a chosen algorithm. A gradient-free algorithm—COBYLA—was used in the present study. The algorithm is intended for constrained problems, and it is part of the open source optimisation library NLopt [5]. A detailed description of the algorithm can be found in [6].

As described in [3], the number of optimisation variables in power management optimisation is scaled directly according to the defined system topology. This means that each unit in the machinery adds one optimisation variable to the problem. The variable is the output power of the unit, which is scaled against its maximum continuous rate (MCR). For the studied fishing boat machinery, the variables are $\hat{P}_{ME}$, $\hat{P}_{M/G}$ and $\hat{P}_{GEN}$. In addition, variant d) has one more optimisation variable for the rotational speed of a CPP. The implementation of the COBYLA algorithm allows for defining the maximum and minimum boundaries for each optimisation variable. In the present study, the variable values are bounded between [0,1].

Optimisation minimises the objective function (Eq. 3), which describes the total fuel consumption rate of all fuel consumers in (Tonne/h). Here, the operating power of the individual component, P_{ME}, $P_{M/G}$ and P_{GEN}, is the scaled optimisation variable multiplied by the MCR of the component. The brake-specific fuel consumption (BSFC) of each combustion unit at a given operating point power is interpolated from its fuel consumption maps.
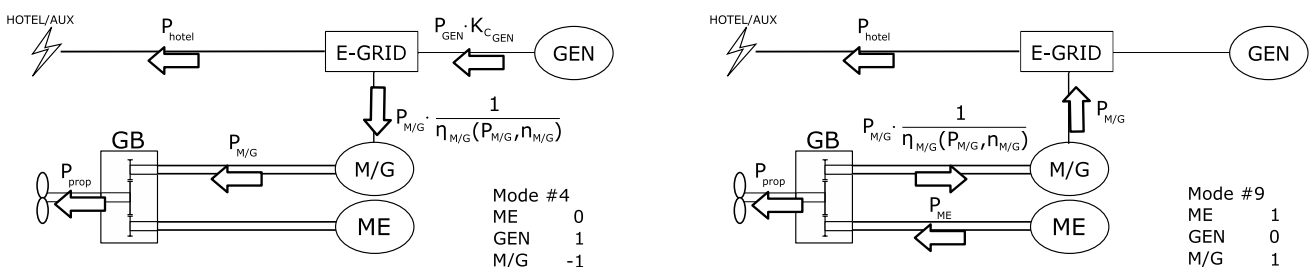
$$\text{BSFC}_{ME}(\hat{P}_{ME}, n_{ME}) \cdot P_{ME} + \text{BSFC}_{GEN}(\hat{P}_{GEN}) \cdot P_{GEN} \quad (3)$$

The constraint functions ensure that the power system is in equilibrium and that the machinery is not overloaded. The propeller equations convert the requested duty cycle into a propeller power demand, $P_{prop,t}$, at a time instant t. The load must be supplied with the machines attached to the gearbox's input shafts, as described in Eq. 4. Because the optimisation variables represent the output power of the component, the coefficient for the gear contact efficiency, K_{GB}, depends on the operating mode of the component. For the ME, this coefficient is a constant 0.98. For the M/G, it is piecewise defined because the unit can transfer power in two directions: the coefficient is 0.98 if the unit is motoring and 0.98^{-1}, if the unit is generating. The internal loss coefficient, K_c, describes the lumped electrical-to-mechanical conversion and distribution losses, which are interpolated from the efficiency maps shown in Fig. 5. For the M/G, this loss coefficient is piecewise defined based on the operating mode because the variable $P_{M/G}$ always describes the output power of the M/G. This does not mean that the M/G operates without losses in the motoring mode but rather that the internal conversion losses are pulled out of the AC grid, which is shown in Eq. 5. Here, the negative sign simply ensures that the summation on the right-hand side of gearbox power equilibrium is correctly affected according to the operating mode of the M/G.

$$P_{prop,t} = P_{ME} \cdot K_{GB_{ME}} - P_{M/G} \cdot K_{GB_{M/G}} \cdot K_{c_{M/G}}$$

$$\text{where } K_{GB_{M/G}} = \begin{cases} 0.98 & \text{motoring} \\ 0.98^{-1} & \text{generating} \end{cases} \quad (4)$$

$$\text{and } K_{c_{M/G}} = \begin{cases} -1 & \text{motoring} \\ \eta_{M/G}(\hat{P}_{M/G}, n_{M/G})^{-1} & \text{generating} \end{cases}$$

Fig. 6 Examples of the discrete mode combinations for the machinery

	All possible mode combinations											
	#1	#2	#3	#4	#5	#6	#7	#8	#9	#10	#11	#12
ME	0	0	0	0	0	0	1	1	1	1	1	1
GEN	0	0	0	1	1	1	0	0	0	1	1	1
M/G	-1	0	1	-1	0	1	-1	0	1	-1	0	1

Similarly, Eq. 5 is used to ensure that the requested load $P_{\text{hotel},t}$ is supplied by the GEN, the M/G or both of them. The combustion unit of the GEN provides the shaft power, P_{GEN}, and the electric output power after the conversion losses equals $P_{\text{GEN}} \cdot K_{c_{\text{GEN}}}$. The conversion losses in the M/G, $K_{c_{\text{M/G}}}$, are piecewise defined, just like in Eq. 4. The losses depend on the operating mode but are now reversed if compared with the gearbox.

$$P_{\text{hotel},t} = P_{\text{GEN}} \cdot K_{c_{\text{GEN}}} - P_{\text{M/G}} \cdot K_{c_{\text{M/G}}}$$

$$\text{where } K_{c_{\text{M/G}}} = \begin{cases} \eta_{\text{M/G}}(\hat{P}_{\text{M/G}}, n_{\text{M/G}})^{-1} & \text{motoring} \\ -1 & \text{generating} \end{cases} \quad (5)$$

$$\text{and } K_{c_{\text{GEN}}} = \eta_{\text{GEN}}(\hat{P}_{\text{GEN}})$$

Each unit in the machinery that has a speed-dependent efficiency map in Fig. 5 also needs a constraint function to describe the speed-dependent maximum limit for the load of the component. These maximum load limits are visible in Fig. 5 as a black line between the coloured contour plot and the white area.

In addition to the constraints shown above, variant (d) needs one more constraint function. Because the algorithm also varies with the value of the CPP speed, Eq. 6 ensures that the requested vessel velocity is achieved. Without this constraint, the gradient-based algorithm might end up in a slope in the optimisation surface, where the propeller speed is decreasing but the propeller pitch is saturated to its maximum value. This slope leads the algorithm to reduce the propeller speed even more because it reduces the propeller load, in turn lowering the fuel consumption for the system's power sources.

$$V = V_{\text{request}} \quad (6)$$

The optimisation routine does a post-processing check for each solution that the COBYLA algorithm returns. This safety measure ensures that the solution indeed respects all the defined constraints and hence is a truly feasible candidate for a local optimum. From all the different local optima that are achieved with the two-layered optimisation routine, the one with the lowest objective function value is picked to represent the best overall solution.

4 Results and discussion

This section presents the simulation results for the studied fishing boat that has the four propulsion variants. The results are presented for the operating points defined in Fig. 4. The machinery operating points are optimised to minimise their total fuel consumption rate. The variations in the propeller operating points are discussed first.

4.1 Propeller operating points for the optimal solutions

When propeller Eqs. 1a –1e convert the velocity request and the resistance from the duty cycle into the propulsion load, the different propulsion variants have different propulsion loads. To show the propeller operating points, Fig. 7 maps the equilibrium points in an open water efficiency graph for each of the studied variants.

As mentioned in Sect. 2, the single-speed CPP and FPP variants both have a single propeller operating point for each vessel's operating point in the duty cycle. In other words, solving the optimisation problem does not affect the operating point of the propeller for variants (a) and (b). Although it is hard to read from Fig. 7a, b, the operating efficiency with the FPP is better in all operating points when compared with the single-speed CPP. The difference mainly comes from the fact that the propeller is operating below its rated power throughout the duty cycle. With the rated propeller speed of 153 rpm, the single-speed CPP finds the equilibrium points at lower P/D ratios compared with the FPP, which leads to lower propeller efficiencies. In other words, the FPP operates at lower speeds. The biggest difference is found at the low-speed transit condition, where the FPP operates at a superior operating point compared with the single-speed CPP.

With the two-speed CPP, TOpti searches for the minimal fuel consumption for both the discrete values for the propeller speed and uses the lower fuel consumption value as the found optimum. In other words, the lower propulsion load does not automatically guarantee lower fuel consumption although in practical solutions and real-life machines, this might be the case. Figure 7c shows the operating points for the CPP with a two-speed gearbox and the colour shows which gear was used for the optimal system operation. The optimal operating points for the two-speed CPP have a wider range when compared with the single-speed CPP points. The change in operating points shows that with the studied machinery and operating conditions in the duty cycle, it is more fuel efficient to use the lower propeller speed (the second gear with a gear ratio of 8.3:1) almost everywhere. The high-speed transit points are moved to a region with a higher efficiency. The operating points for the trawling mode are also scattered more, and although not clearly visible from the graph, the efficiencies have slightly improved. The improvement in the efficiency comes from running the propeller at a lower speed and higher pitch. The higher propeller speed is only used for the point with the highest trawling load, which takes place between the 1 and 1.5 h mark in the duty cycle. It should be noted that the machinery runs at its rated speed regardless of the active gear in the gearbox.
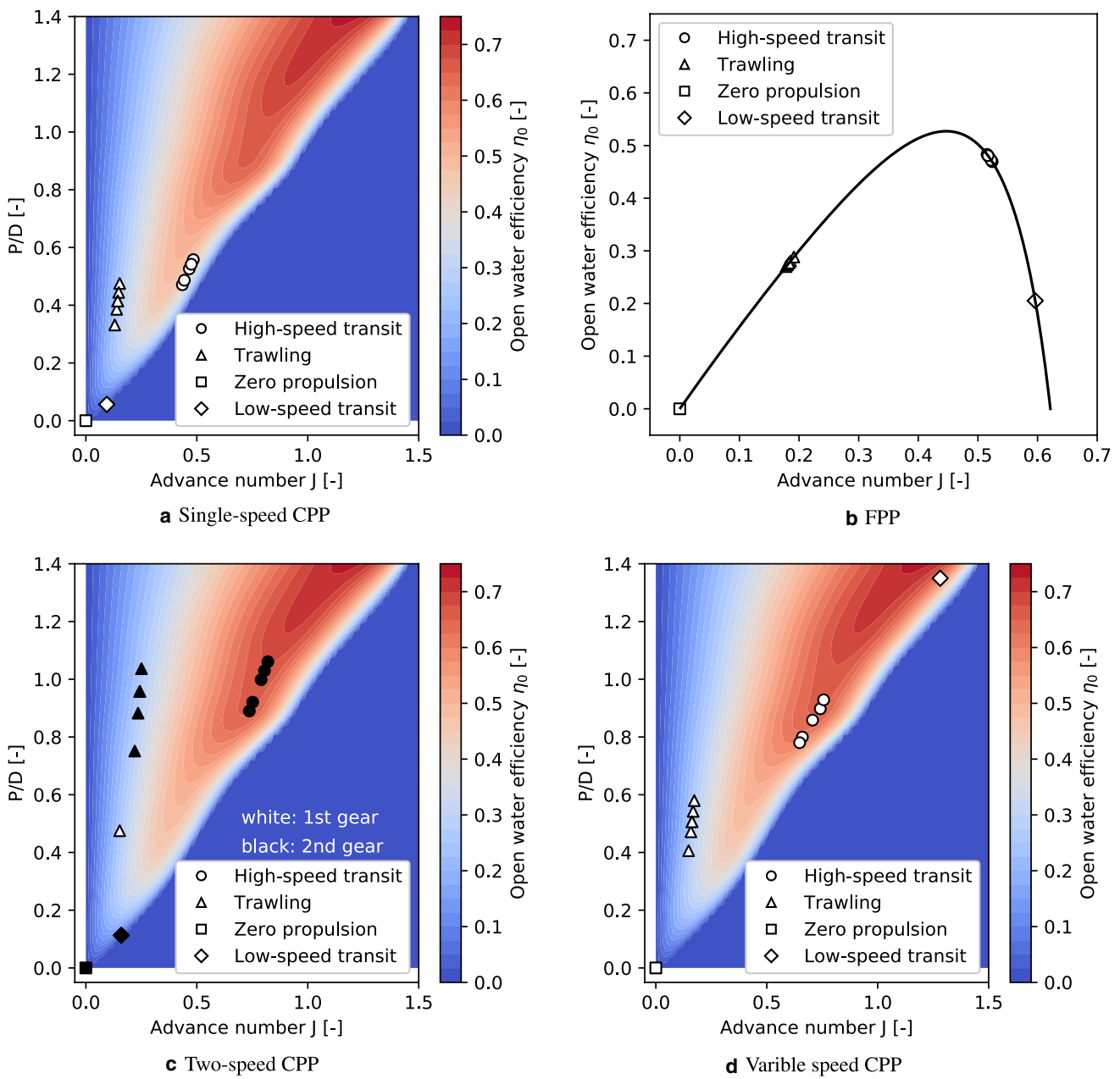
Fig. 7 Propeller operating points in the studied systems

The operating points of the variable-speed CPP are shown in Fig. 7d. Here, the propeller speed is allowed to continuously drop to zero and hence reach higher P/D ratios and potentially higher open water efficiencies. Now, however, the gearbox only has a single reduction speed, meaning that the operating speed of the ME and the M/G change as the propeller speed changes. In other words, although the propeller speed has decreased to reach better propeller operating points, the ME and the M/G move away from their rated speed to speeds with a lower efficiency. Therefore, the high-speed transit points did not move as much as with the

two-speed CPP. Yet the high-speed operating points are at a higher efficiency region compared with the single-speed CPP. The trawling mode operating points of the propeller have moved to slightly lower propeller speeds and higher P/D ratios compared with the single-speed CPP but not as much as with the two-speed CPP. The most interesting point to note here is the low-speed transit, which has moved to a much higher efficiency region. Here, it runs at maximum P/D ratio of 1.35 and only at a speed of 11 rpm.

In conclusion, when it comes to Fig. 7, the propeller's operating points for the different operating modes of the

fishing boat are clustered on the efficiency map. These clusters land on slightly different locations on the map based on the basic principles and characteristics behind the propellers and propulsion variants, but also on the overall optimisation problem of minimising fuel consumption.

4.2 Optimal load shares for the different variants

Next, we look at the optimisation results from the machinery perspective, which are shown in Fig. 8. Figure 8a shows the scaled propulsion and HOTEL/AUX loads, and Fig. 8b–d shows the load shares of the individual components during the duty cycle. The HOTEL/AUX load is common for all

variants. Essentially, the propeller loads in Fig. 8a show the propeller operating points from Fig. 7 in a time frame of the simulation. In Fig. 8, the relative comparison between the variants is easier: because all propulsion variants deliver the same thrust at the equilibrium points, a better open water efficiency into a lower propeller shaft power.

Of all the variants, the single-speed CPP operates at the poorest open water efficiency and, therefore, runs at the highest propeller loads throughout the duty cycle. During the trawling phases, the FPP has the lowest propeller loads, while the two-speed CPP meets the high-speed transit request with the lowest loads. For the two-speed CPP, the shown optimum is found at a lower propeller speed for
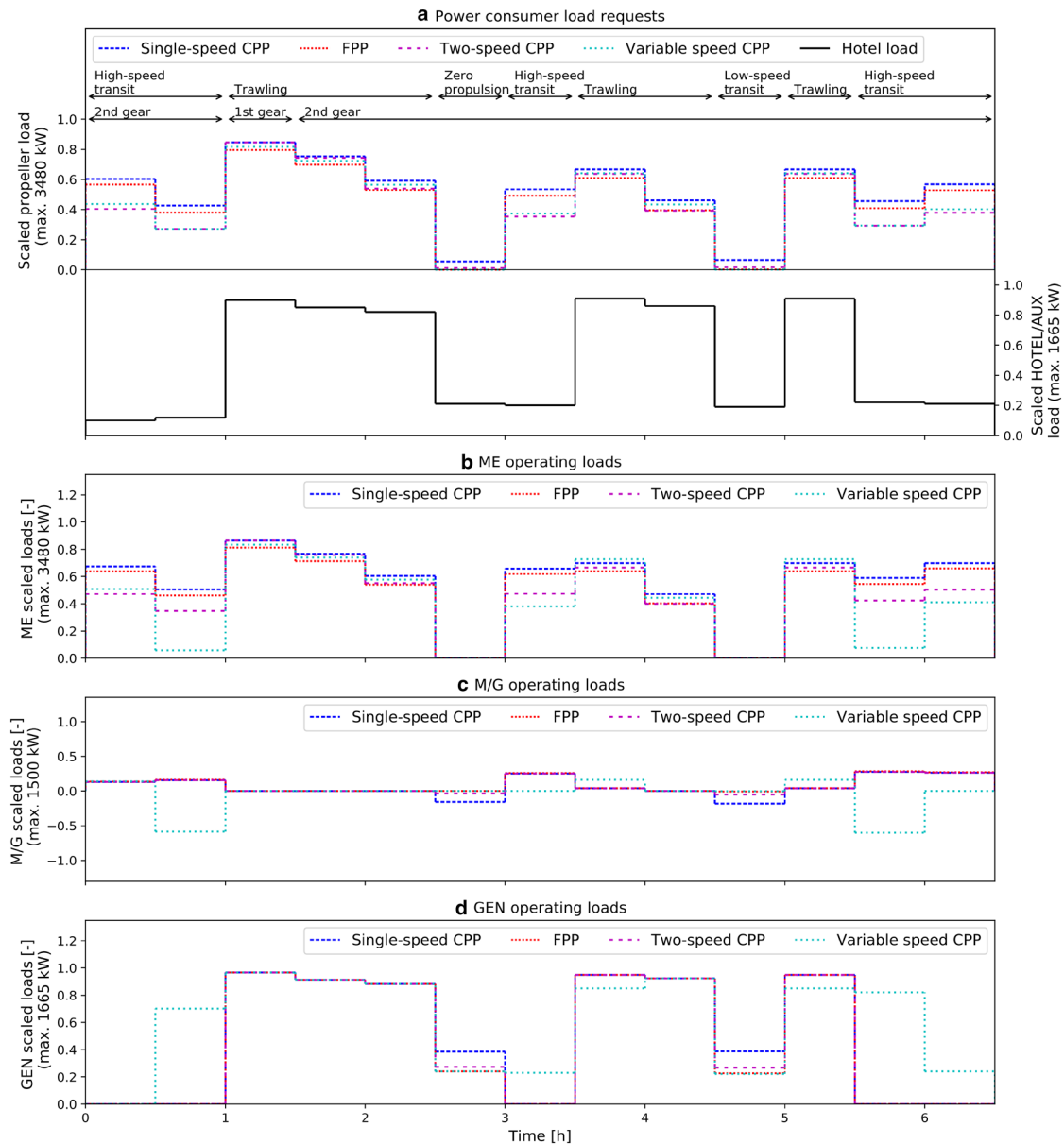

Fig. 8 Propulsion and HOTEL/AUX loads and optimal machinery usage during operation

all other times, except during the heaviest trawling period between the 1 and 1.5 h mark.

None of the variants can clutch off the propeller from the gearbox. To avoid drifting under zero propulsion, the ability to readily generate propulsion is maintained in two ways: the single- and two-speed CPP sets the propller pitch to zero, but the propeller is rotated according to the rated speed of the machinery. For the two-speed CPP, the used gear ratio also affects the idle speed of the propeller. The FPP and the variable-speed CPP can stop the propeller, and its readiness is maintained by having at least one of the power sources active. During the zero propulsion period between 2.5 and 3.0 h, the HOTEL/AUX load is non-zero. Therefore, at least one of the power sources will be active. Figure 8a shows that the FPP and variable-speed CPP are stopped to avoid an idle propeller load. By using the lower propeller speed, the idle load of the two-speed CPP is greatly reduced when compared with the idle load of the single-speed CPP.

The optimal power management of the individual components in the machinery is shown in Fig. 8b–d. For the single- and two-speed CPP and the FPP, the optimal power management is similar in a large-scale setting and hence is discussed first. The high-speed transit periods are powered by the ME and PTO mode, and the GEN is shut off. The low propulsion power requirement in the low-speed transit period is best supplied from the GEN, while the M/G works in the PTI mode, and the ME is shut off. In a similar way, the idle propeller power in the single- and two-speed CPP is generated in the PTI mode during the zero propulsion period. Here, the ME is shut off. The FPP does not have an idle propeller load because the propeller is stopped. Although the ME and M/G are stopped, the PTI is virtually in standby because the GEN is feeding the HOTEL/AUX load. In trawling periods, the propulsion and HOTEL/AUX loads are not shared, but the ME supplies power to the propulsion, and the GEN feeds the electric power consumers, but the M/G is inactive.

Two trawling periods stand out because of their counter-intuitive load shares. Both periods at 3.5–4.0 h and 5.0–5.5 h have the same requests for the vessel's operating point. For these points, the optimal machinery usage shows that the ME is run below its sweet spot (at a 71% load), the GEN is run above its sweet spot (at a 98% load), and the M/G is run at the PTO mode with a very low load (3% load). However, moving the operating points of the ME and GEN closer to their peak efficiencies is not the optimum. This type of load levelling would mean that part of the electric load would be moved from the GEN to the M/G. By doing so, a bigger portion of the electric load would be generated at a poor efficiency which the M/G has at low loads. In other words, the increased energy conversion losses would exceed the small gains achieved from the slightly improved specific fuel consumption. This is highlighted in the example in Fig. 9a, which has a contour plot of the total fuel consumption rate in the machinery, along with the line plots that show where the system is in equilibrium regarding its power. Figure 9a shows the optimisation space for the single-speed CPP where the machinery is running at its rated speeds. The showed constraint plots are only valid for the propulsion and HOTEL/AUX loads at the 3.5–4.0 h and 5.0–5.5 h periods at the rated machinery speeds. Figure 9b shows the total fuel consumption rate along the constraint line. In other words, when walking along the constraint lines of Fig. 9a, the contour values are projected to the x-axis. This closer look shows that the PTO mode with the above-mentioned ME load of 71% is the minimum under these conditions. With propulsion and HOTEL/AUX loads at 3.5–4.0 h, a pure PTO mode where the GEN is shut off is not feasible because of the maximum power capacities of the ME and M/G.
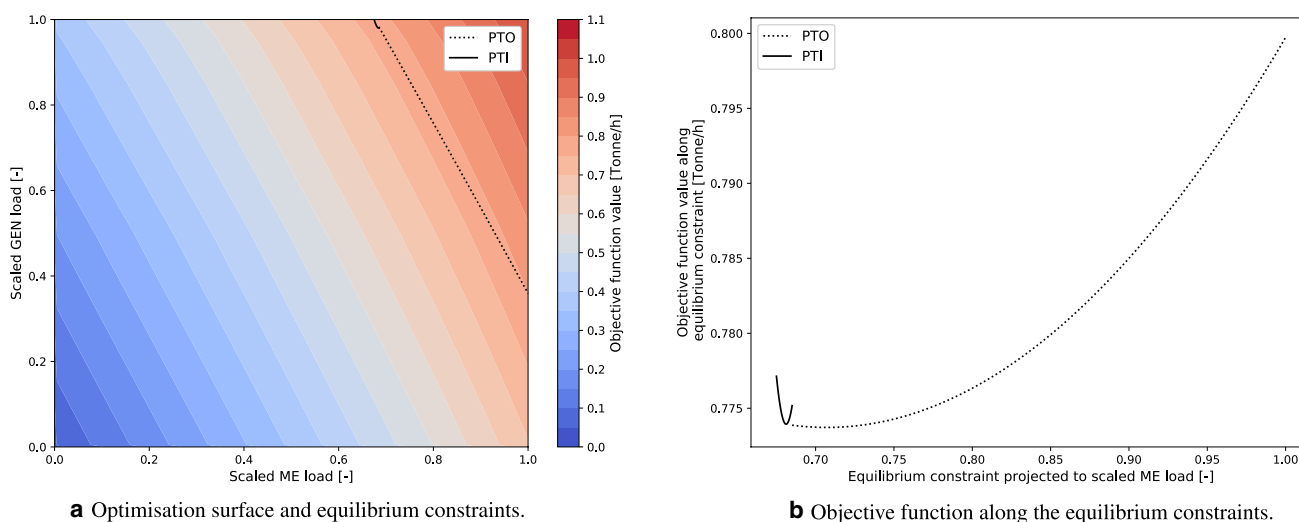

a Optimisation surface and equilibrium constraints.

b Objective function along the equilibrium constraints.

Fig. 9 Objective function values at the rated speed of the machinery at 3.5–4.0 h

The optimal power management with the variable-speed CPP diverges from the other three variants. From a system perspective, there are two main reasons behind this. First, when the propeller speed is reduced to reach better open water efficiency regions, the machinery speed moves away from the rated speed and the best component efficiency. Second, according to the shown power limits in Fig. 5, the reduction in the rotational speed of the machinery reduces the available power from these components. The differences are the most visible in the high-speed transit periods. The time periods between 0.5–1.0 h and 5.5–6.0 h show that most of the propeller power comes from the electric grid: the PTI mode is highlighted by the negative values in the M/G usage. Because the propeller and machinery speed has been reduced, the maximum power limit of the M/G is also reduced, as shown in Fig. 5. The optimum is found at the operating point where the difference in propulsion power and available power from the PTI is filled from the ME. The optimum usage between 3.0–3.5 h and 6.0–6.5 h shows that the M/G is not utilised at all. Hence, the propulsion and HOTEL/AUX loads are supplied from the ME and GEN, respectively.

4.3 Validation with exhaustive search

Unfortunately, the authors of the current article could not validate the presented optimisation methodology with measurement data. However, the results achieved with the proposed LT methodology can be benchmarked using an exhaustive search algorithm, which is classified as a global optimisation algorithm. This section includes two discussions that utilise an exhaustive search algorithm. First, the effect of the propeller speed in variant d) is studied using an array of discrete rotational speeds for the machinery. This is followed by a more systematic study of the load share and propulsion load in all four studied system variants when the two optimisation methodologies are compared.

In simulations, the variable-speed CPP showed sensitivity to the different initial guesses in the optimisation search. Because the used gradient-based optimisation algorithm—COBYLA—searches for the minimum in the multidimensional and constrained optimisation surface, it sometimes ends up with a local optimum. Therefore, it is essential to use different initial guesses for the search. The next example demonstrates how the propeller speed affects the objective function in the variable-speed CPP.

Similar to Figs. 9b, 10 projects the objective function of the variable-speed CPP to the scaled ME load when looking at a feasible operating range, which is set by the constraint equations. The graphs are plotted with discrete rotational speeds for the transit period at 0.5–1.0 h. The contour plots of the optimisation surface are not shown here because each propeller speed has its contour plot for

the objective function value. It also shows the different feasible operating modes for the machinery with different line types and markers. The propulsion request for this time period is achieved using propeller speeds that exceed 66 rpm. At 70 rpm and 80 rpm, the only feasible mode is the PTI mode, where both the ME and the M/G are powering the propeller. This is a result of violating the constraint for the maximum power capacity of the M/G if the HOTEL/AUX load is supplied from the ME and the PTO mode. As the rotational speeds increase, the PTO mode becomes feasible for the studied vessel operating point. As the propeller and machinery speed increase, the maximum capacity of the M/G stops restricting us from feeding also the HOTEL/AUX load from the PTO alone while the GEN is shut off (noted as the discrete points 'PTOpure'). At propeller speeds of 100 rpm, 120 rpm and 140 rpm, the discrete points show that the pure PTO mode is the optimum mode under the studied load condition. The lowest objective function value for the variable-speed CPP was found at a propeller speed of 90 rpm. The lines for 70 rpm and 80 rpm show a steeper slope for the objective function value. However, we cannot extend the lines for 70 rpm and 80 rpm further left because the maximum capacity of the M/G would be exceeded: thus, a higher load share would be required from the ME to supplement the propulsion load. A pure PTI mode where the ME is shut off is not possible because the maximum power of the M/G would be exceeded even more. When using the propeller speed as a continuous variable, the optimum was found at 89.8 rpm with the load shares presented in Fig. 8.

Finally, we run the simulations for the four propulsion variants while using an exhaustive search to find a global optimum for all the variants in a discrete search grid. Full combinatorial search grids are constructed from
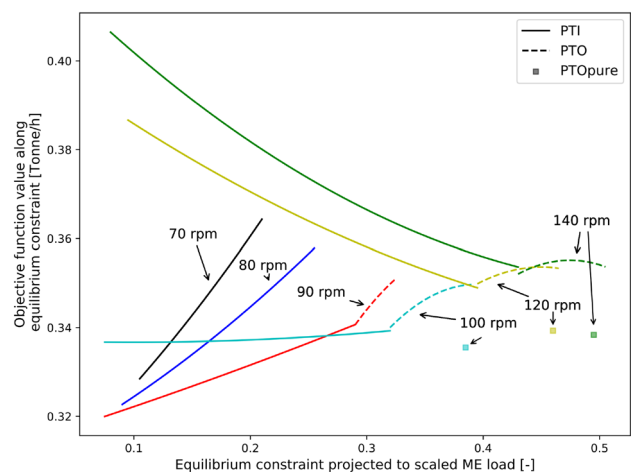

Fig. 10 Projected objective function values for different propeller speeds at time 0.5–1.0 h

the discretised control arrays, which are shown in Eq. 7. It should be noted that the propeller speed array is only used for the search grid in the variable-speed CPP. For the validation, we use the objective and constraint functions described in Sect. 3.

$$u = \begin{cases} \text{ME} : [0\%, 0.2\%, \dots, 99.8\%, 100\%] \cdot 3480\,\text{kW} \\ \text{M/G} : [0\%, 0.2\%, \dots, 99.8\%, 100\%] \cdot 1500\,\text{kW} \\ \text{GEN} : [0\%, 0.2\%, \dots, 99.8\%, 100\%] \cdot 1665\,\text{kW} \\ \text{M/G modes} : [\text{motoring, generating}] \\ n : [10\text{rpm}, 20\text{rpm}, \dots, 150\text{rpm}, 160\text{rpm}] \end{cases}$$
(7)

Figure 11 shows the validation errors during the simulation. All errors are relative to the results achieved with the exhaustive search.

The propeller speed errors (Fig. 11, top) for the single-speed CPP and the FPP are both zero because the propeller speed is not included in optimisation problem. For the two-speed CPP, the error is also zero because the search grid is dense enough to find the optimal control combination with the same gear sequence as shown in Fig. 8a. The optimal propeller speed error for the variable-speed CPP peaks at 9 rpm, which is 6% of the rated propeller speed of 153 rpm.

The M/G usage error $\Delta P_{\text{M/G}}$ in Fig. 11 (middle) reflects the load-sharing error between the gearbox and electric grid. For the single- and two-speed CPP and the FPP, this error is less than 15 kW, which translates into 1% of the MCR or five steps in the discretised control array. Yet the operating modes for these three variants are the same throughout for simulation when using both optimisation methods. The variable-speed CPP, however, has three time steps where the M/G usage is noticeably different. At 3.5–4.0-h mark
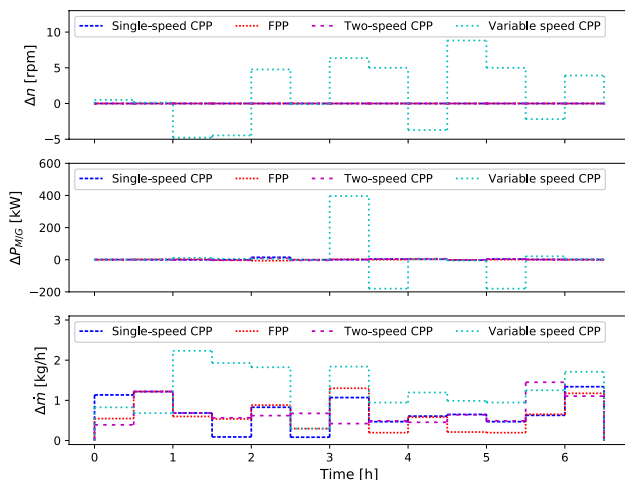
and 5.5–6-h mark, the negative errors mean that the M/G load with an exhaustive search algorithm is smaller than with the LT method. However, the M/G is in generating mode in both of these time instances. The biggest difference in the load-sharing error takes place at the 3.0–3.5-h mark: with the LT method, the M/G was not used at all, while the exhaustive search finds the global optimum at a control that shuts down the GEN and supplies both the propulsion load and the HOTEL/AUX load from the ME. This highlights the earlier discussion in the beginning of Sect. 4.3 regarding the sensitivity of the optimisation search space under varying propeller speeds. The propeller speed array in Eq. 7 is fairly coarse, leading to bigger steps in the propulsion load. Because the exhaustive search algorithm is subject to the curse of dimensionality, the computation times increase exponentially when the length of the arrays in Eq. 7 are increased. With the shown discretisation, the longest simulation (the variable-speed CPP) took 23 h with an Intel i7-7700HQ CPU @2.80 GHz processor, while the same simulation with the author's methodology took 24 min.

The bottom graph in Fig. 11 shows the error in the minimisation target of the optimisation problem: the fuel consumption rate. The errors stay below 3 kg/h, which is equivalent to 0.3% of maximum fuel consumption of the machinery. This results from the fairly flat fuel consumption characteristics of the ME and the GEN. In other words, the errors in load sharing do not have a dramatic effect on the fuel consumption error. The fuel consumption error is positive throughout the simulation, meaning that the values found by the exhaustive search are larger than the ones found with the methodology proposed by the authors. This contradiction, however, is a direct result of the step sizes in the discrete search grid. With discrete step sizes in the grid, an exhaustive search algorithm is not capable of precisely matching the power production according to the requests of the power consumers, which here, leads to excess fuel consumption.

Although a denser grid would be more ideal for validation purposes in an exhaustive search, the used search grid showed that the variable-speed CPP optimisation is the most sensitive variant of the studied propulsion concepts. In addition, the modes in the power management were, for the most part, the same as with the proposed LT method excluding the three load conditions with the variable-speed CPP. Finally, the validation errors were acceptable for the load conditions where the system modes were not affected by step size in the search grid.

4.4 Achieved fuel savings

The top graph in Fig. 12 shows the cumulative fuel consumption of the single-speed CPP as a reference for the fuel savings. The bottom figure shows the difference of the

Fig. 11 Validation errors for propeller speed (top), M/G load (middle) and total fuel consumption rate (bottom)

cumulative fuel consumption for the other variants when compared with the consumption of the single-speed CPP. In other words, the more negative the final value is in the bottom graph, the more fuel the variant has saved compared with the single-speed CPP.

All results highlight that with a CPP, the fuel savings are created by reducing the propeller speed. Significantly, the highest savings are achieved with the two-speed CPP. This is a result of the reduced propeller load, but also because the machinery operates at the rated speed all the time, and the reduction in the propeller speed does not limit the power capacity in the components. The lower propeller speeds reduce the propeller loads, especially during high-speed transit periods. The used FPP has lower propeller loads compared with the single-speed CPP, hence saving fuel. However, the possibility of reaching higher open water efficiency by controlling both the propeller speed and pitch angle, makes the variable-speed CPP a compromise between the FPP and the two-speed CPP.

Finally, we estimate the annual fuel costs and investment costs for the systems and evaluate the payback periods. With the following and assumed unit costs and trip itineraries, we obtain indications of the relative differences between the system costs. All calculations are relative to the single-speed

Fig. 12 The cumulative fuel consumption of the single-speed CPP (top) and the cumulating fuel savings of the other variants (bottom)

CPP. With 200 fishing trips per year and with a fuel cost of $430\frac{\text{Eur}}{\text{Tonne}}$, the annual fuel savings are $200\frac{\text{trip}}{\text{year}} \cdot (3452.6\frac{\text{Tonne}}{\text{trip}} - 3070.6\frac{\text{Tonne}}{\text{trip}}) \cdot 430\frac{\text{Eur}}{\text{Tonne}} = 32852\frac{\text{Eur}}{\text{year}}$ for the two-speed CPP. With equal unit fuel cost and number of annual trips, the annual savings with the FPP are $200\frac{\text{trip}}{\text{year}} \cdot (3452.6\frac{\text{Tonne}}{\text{trip}} - 3324.8\frac{\text{Tonne}}{\text{trip}}) \cdot 430\frac{\text{Eur}}{\text{Tonne}} = 10,991\frac{\text{Eur}}{\text{year}}$ and for the variable speed CPP $200\frac{\text{trip}}{\text{year}} \cdot (3452.6\frac{\text{Tonne}}{\text{trip}} - 3265.8\frac{\text{Tonne}}{\text{trip}}) \cdot 430\frac{\text{Eur}}{\text{Tonne}} = 16065\frac{\text{Eur}}{\text{year}}$.

By approximating the costs for the components, which must be updated between the different topologies, we can conclude the financial estimations by calculating the payback periods when they are compared with the single-speed CPP. The following approximations are used: $100\frac{\text{Eur}}{\text{kW}}$ for the VFD unit, $40\frac{\text{Eur}}{\text{kW}}$ for a single-speed gearbox, $48\frac{\text{Eur}}{\text{kW}}$ for a two-speed gearbox, $100\frac{\text{Eur}}{\text{kW}}$ for a CPP and $80\frac{\text{Eur}}{\text{kW}}$ for an FPP. Because the two-speed CPP only needs to replace the gearbox, the payback period is relatively short, $(48\frac{\text{Eur}}{\text{kW}} - 40\frac{\text{Eur}}{\text{kW}}) \cdot 3480\,\text{kW}/32,852\frac{\text{Eur}}{\text{year}} = 0.9$ years. For the FPP and variable-speed CPP, the VFD unit is added in the system, which increases the payback periods for the systems. On the other hand, a CPP is more expensive to manufacture because an additional mechanism is required to change the propeller pitch angle. With an additional VFD cost and a reduced propeller cost, we obtain a payback period for the FPP: $(100\frac{\text{Eur}}{\text{kW}} \cdot 1500\,\text{kW} + (80\frac{\text{Eur}}{\text{kW}} - 100\frac{\text{Eur}}{\text{kW}}) \cdot 3480\,\text{kW})/10,991\frac{\text{Eur}}{\text{year}} = 7.3$ years. For the variable speed CPP, we obtain $100\frac{\text{Eur}}{\text{kW}} \cdot 1500\,\text{kW}/16,065\frac{\text{Eur}}{\text{year}} = 9.3$ years. The fuel consumptions, savings and payback periods are summarised in Table 3.

5 Conclusion
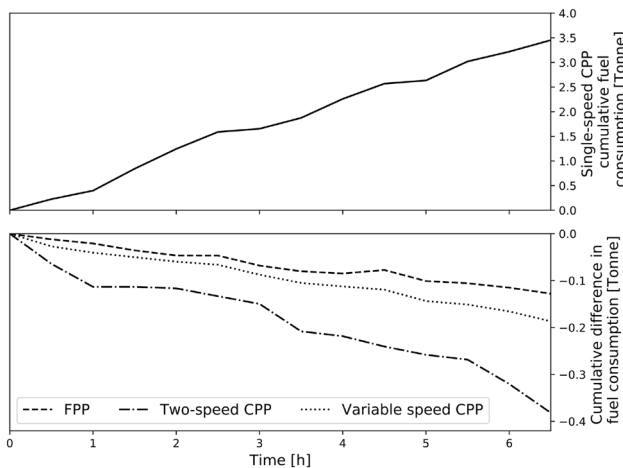
The current article presented a comparison of the different propulsion variants for a fishing boat and optimised the machinery usage for each variant using a recently developed optimisation tool: TOpti. The described tool aims to serve the needs of system integration engineers in the marine industry; with its low level of details and static

Table 3 Summary of the results

| Propulsion variant | Fuel consumption [$\frac{\text{kg}}{\text{trip}}$] | Fuel saving [$\frac{\%}{\text{trip}}$] | Annual fuel save [Eur] | Investments relative to the single-speed CPP [Eur] | | | | Payback time (years) |
				Propeller	Gearbox	VFD	Total	
Single-speed CPP	3452.6	0.0	0.0	0.0	0.0	0.0	0.0	–
FPP	3324.8	3.7	10,991	− 69,600	0.0	150,000	80,400	7.3
Two-speed CPP	3070.6	11.1	32852	0.0	27,840	0.0	27,840	0.9
Variable-speed CPP	3265.8	5.4	16,065	0.0	0.0	150,000	150,000	9.3

system modelling, it offers engineers a time-efficient way to optimise and compare complex machinery configurations without having to define the optimisation problem itself.

The optimisation problem minimised the fuel consumption of the fishing boat over a generic duty cycle. When an FPP was compared with a single-speed CPP that had similar characteristics, the fuel consumption improved. The results showed that a reduction of the propeller speed with a CPP, either using a two-speed gearbox or continuously with the rotational speed of the machinery, improved the fuel efficiency of the machinery even more. The two-speed CPP showed the best fuel savings—11%—because the propeller load during high-speed transit periods was reduced, yet the machinery could still be operated at its rated speeds. The results with the proposed optimisation methodology were validated using an exhaustive search algorithm.

The current article continued describing the energy management optimisation capabilities of the developed optimisation framework. The possibility of including different propeller types and propulsion control variants increases the versatility of the tool already at the current stage but even more so in future, when the higher-level design optimisation features will be included in the methodology.

References

1. Geertsma R, Negenborn R, Visser K, Hopman J (2017) Design and control of hybrid power and propulsion systems for smart ships: a review of developments. Appl Energy 194:30–54
2. Jaurola M, Hedin A, Tikkanen S, Huhtala K (2019) Optimising design and power management in energy-efficient marine vessel power systems: a literature review. J Mar Eng Technol 18(2):92–101. https://doi.org/10.1080/20464177.2018.1505584
3. Jaurola M, Hedin A, Tikkanen S, Huhtala K (2018) Topti: a flexible framework for optimising energy management for various ship machinery topologies. J Mar Sci Technol. https://doi.org/10.1007/s00773-018-0617-4
4. Carlton J (2012) Marine propellers and propulsion. Butterworth-Heinemann, Oxford, p 81. https://doi.org/10.1016/C2010-0-68327-1
5. Johnson S (2014) The nlopt nonlinear-optimization package, http://ab-initio.mit.edu/nlopt. Accessed 12 Nov 2018
6. Powell MJD (1994) A direct search optimization method that models the objective and constraint functions by linear interpolation. In: Gomez S, Hennart JP (eds) Advances in optimization and numerical analysis. Mathematics and its applications, vol 275. Springer, Dordrecht. https://doi.org/10.1007/978-94-015-8330-5_4